Hindawi
Advances in Civil Engineering
Volume 2023, Article ID 5213452, 14 pages
https://doi.org/10.1155/2023/5213452

Research Article

Seismic Reduction Performance of Wrap Rope Connection Devices for Continuous Girder Bridges

Yanfang Liu,[1,2] **Wenxue Zhang**,[1] **Xiuli Du**,[1] **and Weigang Bao**[2]

[1]*College of Architecture and Civil Engineering, Beijing University of Technology, Beijing 100124, China*
[2]*China Communications Construction Company Limited, Beijing 100088, China*

Correspondence should be addressed to Yanfang Liu; liuyanfang1@ccccltd.cn

Received 18 August 2022; Revised 19 September 2022; Accepted 24 November 2022; Published 7 March 2023

Academic Editor: Wei He

In this article, wrap rope connection device (WRCD), which considers the relative acceleration of piers and beam as a control variable, is proposed for improving the current situation of continuous girder bridges whose bearing force of a single pier is along the longitudinal direction and based on the synergy principle. The WRCD device, which meets the slow displacement requirements of temperature and vehicle load under normal operation, is implemented and used to improve the performance of the sliding bearing pier. During earthquakes, because of the amplification effect of the wrap rope, the instantaneous large stiffness state in the longitudinal force can be achieved. Based on the shaking table test of a typical continuous girder bridge for examining the performance of the WRCD during earthquakes, the dynamic characteristics, structural acceleration, displacement, and strain responses of the structure under different frequency spectra, and seismic input intensities are analyzed and the seismic reduction performance of the WRCD is demonstrated. This analysis demonstrated that, by activating WRCD, the ratio of the acceleration response of the fixed bearing pier to the sliding bearing pier increased from 10% to 57%; moreover, the force on each pier appeared more uniform. Furthermore, with an increase in the input intensity of the earthquake, the displacement of the primary beam and the seismic response of the fixed pier bottom considerably decreased and the synergy effect of each pier was more prominent. Under certain site conditions, the WRCD can effectively improve the synergy effect between the sliding bearing piers and fixed bearing pier; however, the improvement in the obtained result is directly associated with the seismic input characteristics. The design parameters of the WRCD should be determined as per different site conditions and the optimum application range of the WRCD.

1. Introduction

Continuous girder bridges are bridge structures commonly used in practical engineering. They account for >40% of the total length of bridges in China. Moreover, in recent years, the construction of continuous girder bridges has shown a gradually increasing trend in quantity and the span of such bridges has steadily increased. The number of spans between the expansion joints has increased from 3-4 to 10–12, and the length of expansion joints are large. With an increase in span and expansion joint length, the design status has not sufficiently changed for the single-fixed bearing to meet the displacement requirement caused by temperature and vehicle load along the longitudinal direction. During earthquakes, the longitudinal seismic load of the superstructure is almost completely held by the single-fixed bearing pier, and the seismic potential of the sliding bearing piers is not completely utilized with the same structural size [1]. Although the ductility of fixed bearing piers can improve the aseismic performance of structures by increasing the reinforcement ratio, this method requires to inevitably produce certain damage in the structure, which is challenging to repair. The most common method to improve the seismic performance of the continuous girder bridges is by installing multiple isolation devices. Researchers have performed substantial research on installing isolation bearings and viscous dampers for continuous beam bridges and obtained considerable research results [2–8]. Kelly and

Eidinger [9] and Kelly [10] proposed the system theory and design method of laminated rubber bearing and performed tensile test research on their approach. Tyler and Robinson [11], Hwang et al. [12], and Abe et al. [13] performed tests on lead-core rubber bearings and obtained the equivalent linear model and hysteretic energy dissipation performance of lead-core rubber bearings. Peng et al. [14] and Zhang et al. [15] examined the seismic behavior of hyperboloid spherical supports. Ou et al. [16], Yan et al. [17], and Shen et al. [18] developed new composite metal dampers and examined their performances. The abovementioned research results provide a foundation for the research and design of bridge damping and isolation. However, no matter what type of damping and isolation device is adopted, a large relative displacement should be employed to achieve the ideal damping effect.

However, irrespective of the dampers and energy dissipation devices used, the ideal energy dissipation performance can be achieved only under large relative displacement between the beam and piers, and the initial stiffness of the energy dissipation devices does not match that of the fixed bearing. Therefore, the aseismic performance of the sliding bearing piers is not completely utilized, and the condition for the single-fixed bearing pier loaded alone has not been fundamentally changed. In recent years, some researchers have conducted systemic research on lock-up devices. However, these devices do not effectively reduce the seismic response of low piers [19, 20]. Owing to the challenges in price and maintenance, they do not have several applications in practical engineering.

Based on the synergy principle on which the wrap rope connection device (WRCD) is proposed, the seismic reduction performance of the WRCD under strong earthquakes has been examined through the shaking table test of a typical continuous beam bridge. The WRCD, which considers the relative acceleration of piers and beams as a control variable, is proposed in this study to improve the current situation of continuous girder bridges whose bearing force of a single pier is along the longitudinal direction and is based on the synergy principle. The WRCD is implemented and used to improve the performance of the sliding bearing pier. The study of different frequency spectra and input intensities were analyzed to reveal the seismic reduction performance of the WRCD through the dynamic characteristics, structural acceleration, displacement, and strain responses of the structure. This result provided a reference for its application in similar bridge structures.

2. Design of WRCD

The WRCD structural diagram is shown in Figure 1. Under normal operation conditions, the WRCD can meet the requirements of slow displacement of the temperature and vehicle load. During earthquakes, the relative acceleration between piers and the beam is considered the controlling variable to activate the rotating inertial force of the mass block, which is attached to the rotating shaft. Greater friction is then generated, which is amplified by the loops of wrap rope through the friction shaft and causes large instantaneous stiffness in the sliding bearing piers and attains the "Lock-up" state. The seismic inertial force of the superstructure is shared between the sliding bearing piers and the fixed bearing pier. Thus, the seismic response of the fixed bearing pier and the longitudinal displacement of the beam ends are reduced. When the input energy of an earthquake is considerable, certain energy can be consumed by the frictional force of the wrap rope, and seismic reduction performance is achieved. The WRCD comprises a rotating shaft ①, additional mass block ②, device backing plate ③, support plate ④, leg ⑤, winding cable ⑥, friction shaft ⑦, and assembly bolt ⑧. The WRCD is proposed based on the principle that uses the friction between the rope and wooden pile to form a self-locking system. When there is a relative movement trend, it can produce considerable friction.

3. Design of Shake Table Tests

3.1. Material Selection. There are multiple materials suitable for developing shaking table test models. Owing to the influence of material selection on the test results, the examination of the mechanical properties and selection criteria of the materials that are selected in the tests is necessary. The materials used vary as per the purposes of the tests. For example, elastic materials, such as steels and plexiglass, are generally used to study the response rules of structures, and elastic-plastic materials, such as concretes, are typically used to examine the damage characteristics and failure modes of structures.

The purpose of the shaking table test is to study the seismic reduction performance of the WRCD during earthquakes and to analyze the dynamic characteristics, acceleration, displacement, and strain responses of the structure under different frequency spectra and input intensities of earthquake excitation. The main beam and piers are composed of the steel material Q345D.

3.2. Similarity Coefficients. Determining three independent similarity coefficients as the primary similarity ratio in the shaking table test model design is usually necessary, and the similarity ratio of other physical quantities can be deduced using the basic similarity ratio. In practice, owing to the limitations of laboratory conditions and model materials, all physical quantities cannot be guaranteed to satisfy the similarity ratio. Therefore, we can obtain certain deduced similarity coefficients, the basic similarity coefficients of the design model, and other similarity coefficients of different physical quantities.

The maximum weight of the shaking table is 20 t and the size is 3 m × 3 m. The similarity coefficient of the length of the model is 1/30, which is affected by the size and the maximum bearing capacity of the shaking table. The similarity coefficient of acceleration is set to one. As the main beam and piers of the original structure are concrete materials, the similarity coefficient of the elastic modulus is 6.338. The similarity coefficients of other physical quantities

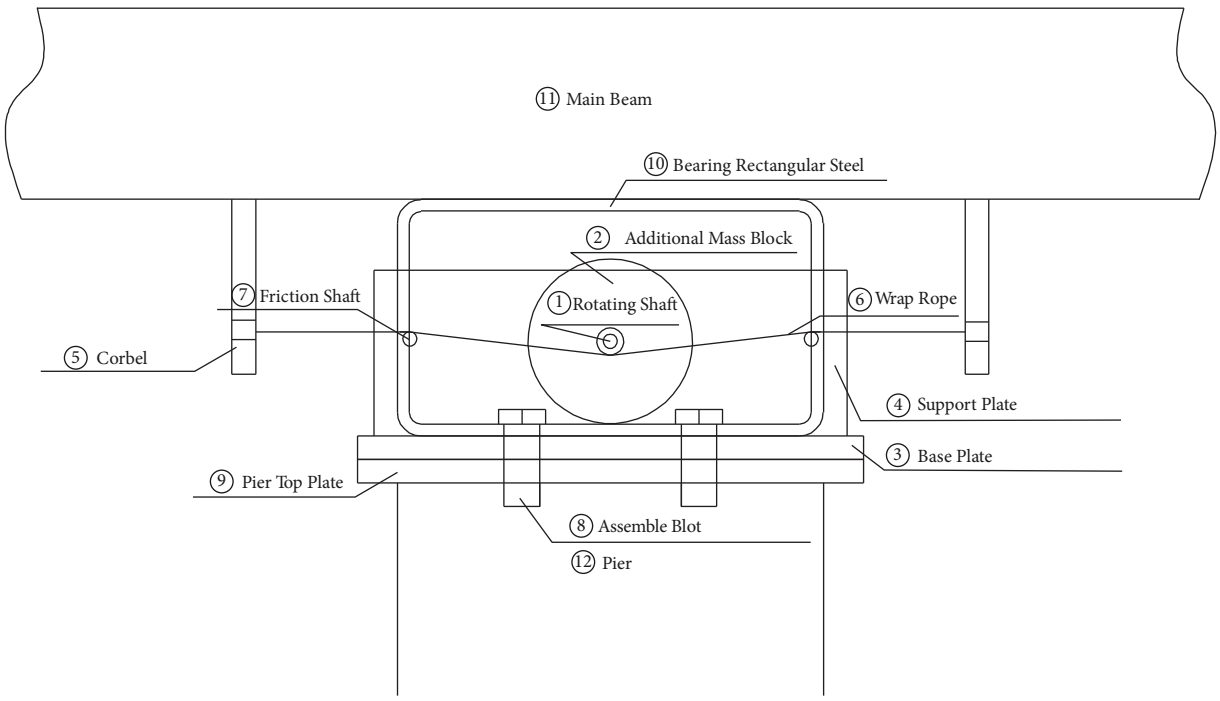

Figure 1: Wrap rope connection device structural diagram.

are derived using these three similarity coefficients. Table 1 lists the similarity ratio of each physical quantity.

3.3. Model Design. Based on the research of a typical continuous girder bridge with a span of $40.55 + 72 + 40.55$ m, a scale model was designed as per the aforementioned similarity ratio. For the shaking table test, the piers were considered as per the equal pier height. The height of the pier was designed as per the geometric similarity coefficients, and the section of the piers was designed as per the equivalent bending stiffness, which neglected the torsional stiffness and compressive stiffness; therefore, the rectangular pipe section was adopted for the simulation. The design parameters of the bridge piers are shown in Table 2. The main beam was modeled as a box section welded by channel steel 20B and steel plates.

3.4. Bearing Design. Four unequal edge angle steel were fixed with the ear plate at the bottom of the main beam and the bolt rod at the top of the piers to model the fixed support. The short leg of the unequal edge angle steel was fixed with the pier using M15 bolts, and the long leg was connected to the ear plate of the main beam using M12 bolts, as shown in Figure 2. The sliding bearing was designed using the integration of the support and WRCD. The base plate of the WRCD was fixed using a pre-embedded bolt rod at the top of the pier, and the sliding bearing was modeled as a polytetrafluoroethylene plate fixed between the $180 \times 100 \times 5\,\text{mm}^3$ rectangular steel plates arranged on the left and right sides of the base plate of the WRCD and the main beam, as shown in Figure 3.

Table 1: Similarity coefficients of every physical quantity (prototype/model).

Physical quantity	Similarity coefficient
Length (L)	1/30
Displacement (δ)	1/30
Elastic modulus (E)	6.338
Stress (σ)	6.338
Density (ρ)	190.154
Velocity (v)	0.183
Acceleration (a)	1
Time (t)	0.183
Frequency (f)	5.48
Stiffness (k)	0.211

3.5. Counterweight Design. Inertial force is the essential factor for the dynamic response of the structure [21–28] and inertial force, which has a causal relationship with the mass. Therefore, in the shaking table test, to accurately simulate the dynamic response characteristics of the model structure during earthquakes, the similarity in equivalent mass between the prototype structure and the model structure is an inevitable factor to be considered. As per the similarity criterion, the model material requires high density; however, the material itself cannot be realized. Therefore, manually adding mass is required for ensuring that the structure meets the quality similarity conditions.

This model uses a counterweight block to add mass. The mass of the counterweight block was divided into 5 and 10 kg, and the actual counterweights of the main beam and pier were 840 and 400 kg, respectively, as shown in Table 3.

Table 2: Comparison of replacement parameters of pier material.

	E (N/mm^2)	I_x (mm^4)	I_y (mm^4)	EI$_x$	EI$_y$
Prototype pier	3.250×10^4	2.310×10^{14}	9.760×10^{13}	—	—
Design	2.060×10^5	2.810×10^6	11.875×10^5	5.790×10^{11}	2.446×10^{11}
Actual	2.060×10^5	2.5520×10^6	8.477×10^5	5.260×10^{11}	1.746×10^{11}

Figure 2: Connection of fixed bearing pier.

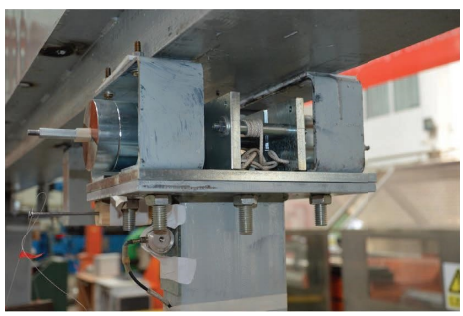

Figure 3: Connection of sliding bearing pier.

Table 3: Additional weight details.

Location	Prototype quality (t)	Model quality (kg)	Model deadweight (kg)	Calculate counterweight (kg)	Actual counterweight (kg)
Beam	5594.2	924.5	167.7	756.8	840
Pier	2116.69	349.8	16.2	333.6	400
Sum	7710.89	1274.3	183.9	1090.5	1240

3.6. Measuring Point Layout. The layout of measuring points primarily considers the dynamic characteristics, seismic response of the structure and stress, and deformation of key parts. A total of thirty-seven sensors were arranged in the entire bridge to test the dynamic characteristics and the seismic response of the structure. The layout of each sensor is shown in Figure 4. Among them were four pull-wire displacement sensors for measuring the absolute displacement of the main beam and pier top. There were five accelerometers to measure the acceleration at the beam end, pier top, and tabletop. There were four strain flowers (three channels for each strain flower), and 16 strain gauges were symmetrically arranged at the pier bottom to measure the strain.

4. Results and Discussion

Four ground motion records, namely, 1976 Qian An (EW), 1940 EL Centro (NS), 1952 Taft, and 1976 Tian Jin (NS), were selected as the seismic loading for different frequency spectra. The test ground vibration input is directly selected to represent the typical measured seismic records of different site types for shaking table tests. The selected measured seismic recording waves are the Qian'an wave with a duration of 21.93 s and the peak of 97.36 gals for the Class I sites; the El-Centro wave with a holding time of 53.73 s and a height of 341.7 gals for Class II sites; Taft wave with a holding time of 54.38 s and a peak of 175.83 gals for Class III sites; and Tianjin wave with a holding time of 19.19 s and

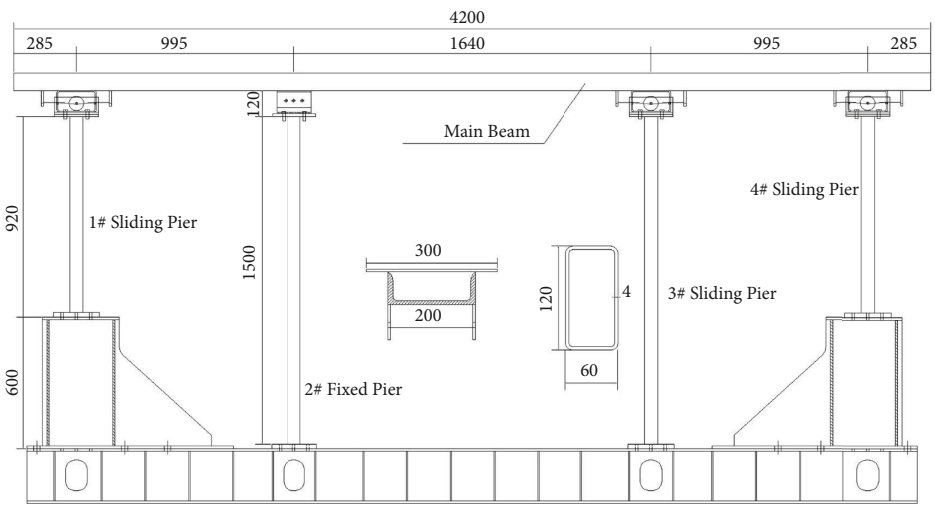

Figure 4: Layout of measuring points.

a height of 145.8 gals for Class IV sites. The Seismo Signal program is used to modify selected time histories such that the peak acceleration and period are compatible with the similarity coefficients. Figure 5 shows the time history used in the test for selected ground motion, and Figure 6 shows the response spectra for a selected ground motion for a 5% damping level.

4.1. Acceleration Responses. Figures 7–10 show the variation trend of the peak acceleration of each pier with different seismic input intensities under the action of EL Centro. For the sliding bearing piers, the maximum acceleration response value of the piers with WRCD decreases more than that without WRCD. For the fixed bearing pier, the maximum acceleration response value with WRCD increases compared to that without WRCD. The results demonstrated that when the WRCD is activated, the sliding bearing piers share the longitudinal seismic force of the superstructure, which is originally subjected to the fixed bearing piers.

Figure 11 shows the columnar comparison of the maximum acceleration response value of each pier with and without WRCD for a seismic peak acceleration of EL Centro wave of 0.4 g. The figure shows that after the WRCD was activated, the longitudinal overall stiffness of the structure increased, and the maximum acceleration response value of each sliding bearing piers decreased by 25%. The maximum acceleration response value of the fixed bearing pier increased by ~4.6 times.

The response of each pier tends to be uniform. The maximum acceleration response value of a fixed bearing pier without WRCD was ~10% of the maximum response value of the sliding bearing pier. After the WRCD was activated, the maximum acceleration response value of the fixed bearing pier was ~57% of the maximum response value of the pier with the sliding bearing pier.

4.2. Dynamic Characteristics. The test model is divided into two types: with and without WRCD. The basic period of the model structure can be obtained using the transfer function. Before each working condition, the structure is swept by white noise to measure the natural vibration rate of the model to determine whether the dynamic characteristics of the structure have changed. Table 4 shows the variation trend of dynamic characteristics of the two models under different working conditions. For the steel structure, the natural frequency of the structure slightly changes, indicating that the structure is still in the elastic stage with and without WRCD. Compared with the test model without WRCD, the natural frequency of the structure is reduced after using WRCD because there are five counterweights on both sides of the device. Owing to the increase in mass, the natural frequency of the model with WRCD is smaller than that without WRCD. The natural frequency with WRCD increases after a peak acceleration of 0.4 g, which demonstrates that with the change in ground motion input intensity, the dynamic characteristics of the bridge structure with WRCD changes, the function of the device considerably improves, and the overall performance of continuous girder bridges can be improved.

4.3. Displacement Responses. Figures 12–15 show the variation trend of the maximum displacement at the sliding bearing piers and the girder with the different seismic input intensities under the action of EL Centro. For the sliding bearing piers, the maximum displacement response value of each pier with WRCD generally increased compared to that without the WRCD. The displacement of the 1# sliding bearing pier increased by 33% on average, the 3# sliding bearing pier increased by 87% on average, and the 4# sliding bearing pier increased by 61% on average. The maximum displacement response value of WRCD was lower than that without the device for the 2# fixed bearing pier, with an average decrease of 31%.

For each sliding bearing pier without the device, the changing range of the maximum displacement response value of piers with the seismic input intensity was relatively less. When the peak acceleration was 0.1~0.4 g, the difference

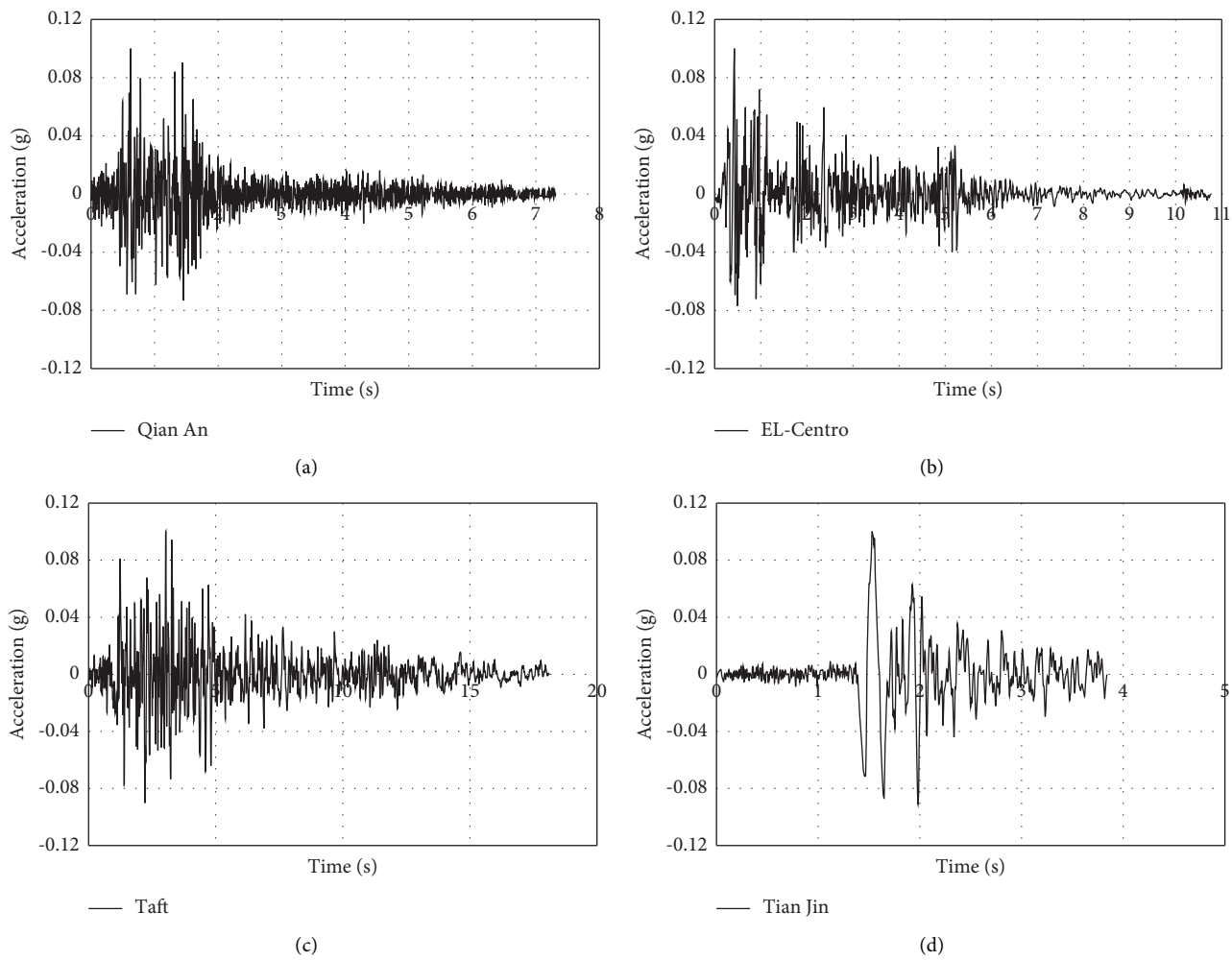

Figure 5: Time history curve of different ground motions: (a) Qian An, (b) EL-Centro, (c) Taft, and (d) Tian Jin.

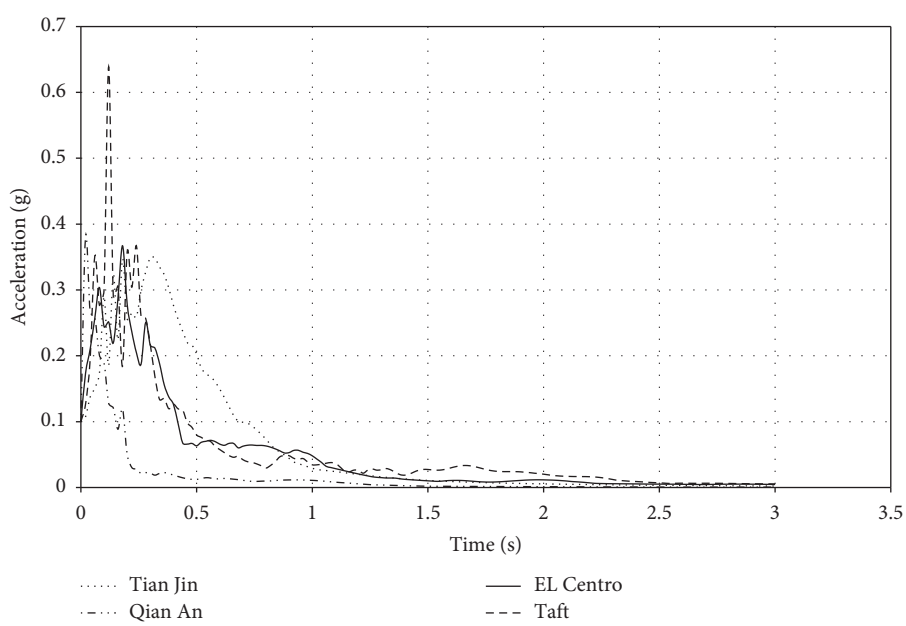

Figure 6: Response spectra of acceleration.

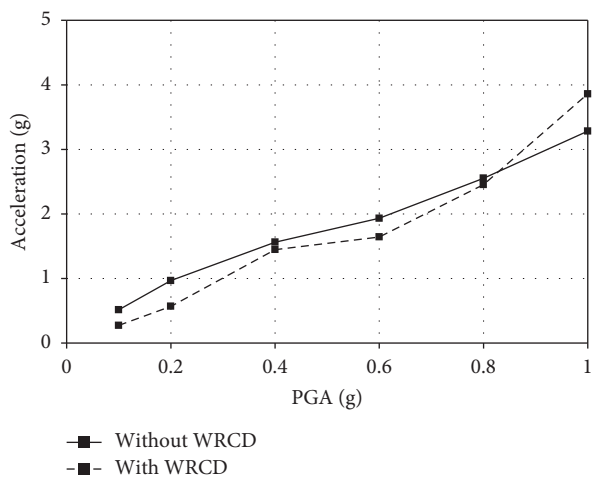

Figure 7: Maximum acceleration of 1# sliding pier top.

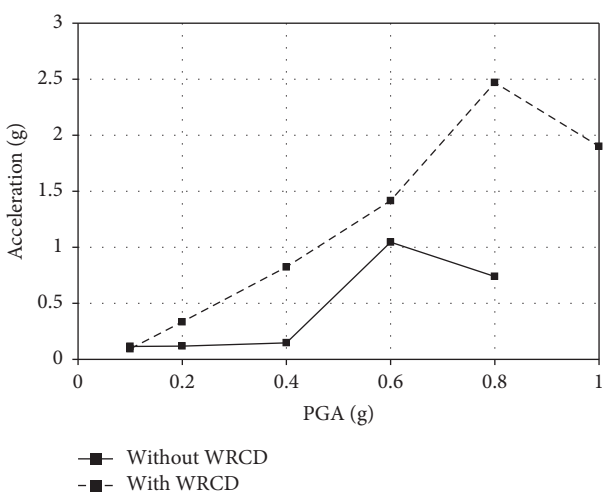

Figure 8: Maximum acceleration of 2# fixed pier top.

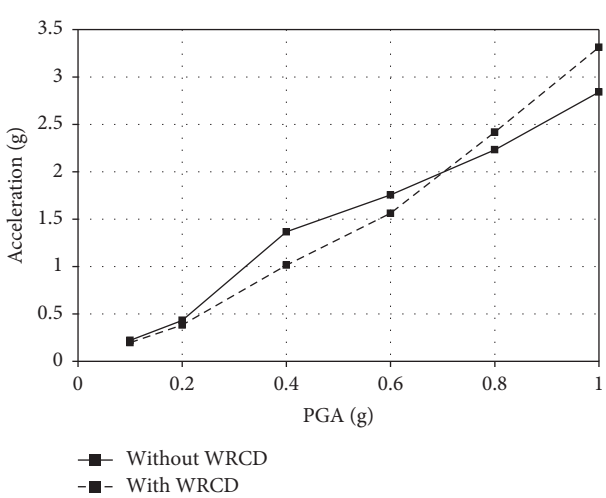

Figure 9: Maximum acceleration of 3# sliding pier top.

between the maximum displacement response values of the two models was small. The maximum displacement response value of piers with WRCD rapidly increased with the change

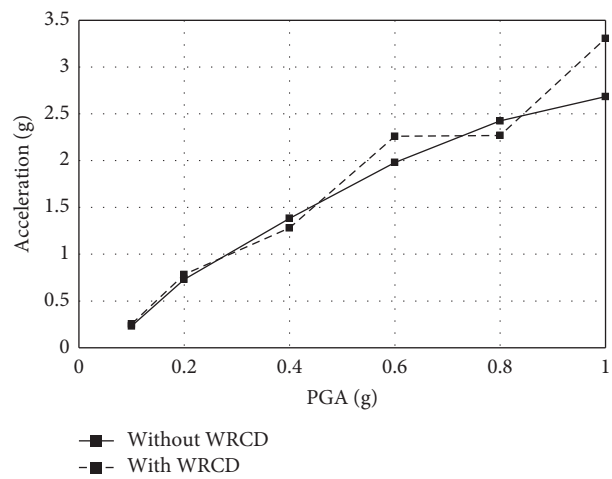

Figure 10: Maximum acceleration of 4# sliding pier top.

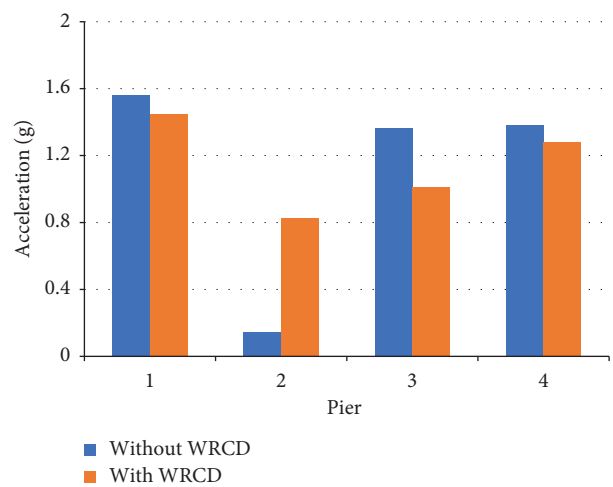

Figure 11: Maximum acceleration of pier top under El Centro input.

Table 4: Natural frequency of the two-test model.

Working condition	Without WRCD (Hz)	With WRCD (Hz)
Before loading	3.654	3.197
0.1 g	3.652	3.194
0.2 g	3.657	3.205
0.4 g	3.652	3.194
0.6 g	3.651	3.248
0.8 g	3.649	3.250
1.0 g	3.655	3.250

in seismic input intensity when the peak acceleration was between 0.6 and 1.0 g, for the setup without the device. The maximum difference in displacement between the two models was large. This demonstrates that when the WRCD is activated, the sliding bearing piers participate in the longitudinal force of the structure and share part of the inertial force of the main beam. With increasing seismic input intensity, the performance of WRCD is more prominent and the overall performance of the continuous girder bridge can be improved.

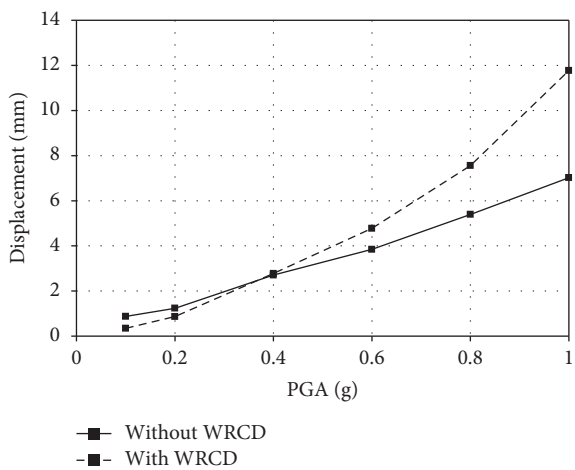

Figure 12: The maximum displacement of 1# sliding pier top.

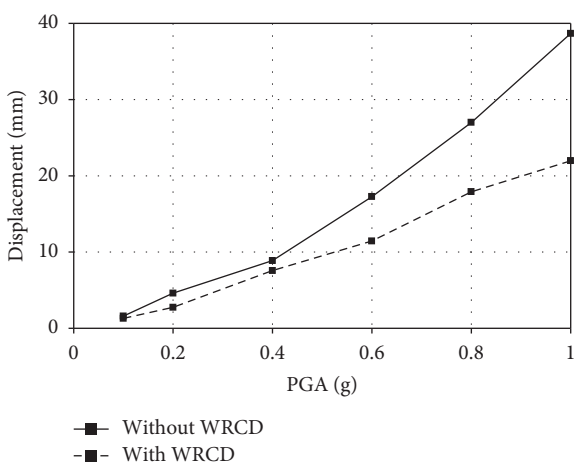

Figure 13: The maximum displacement of 2# fixed pier top.

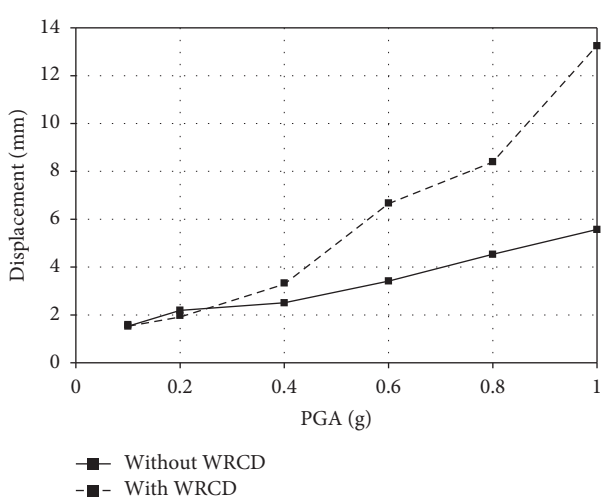

Figure 14: The maximum displacement of 3# sliding pier top.

4.4. Strain Responses. Figures 16–19 show the variation trend of the maximum strain response at the bottom of each pier with different seismic input intensities under the action

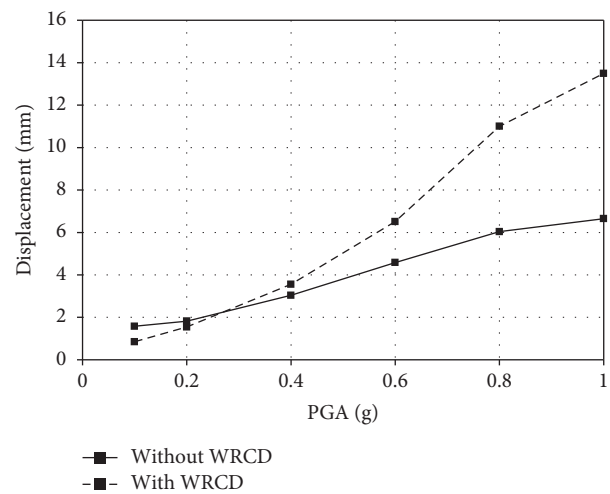

Figure 15: The maximum displacement of 4# sliding pier top.

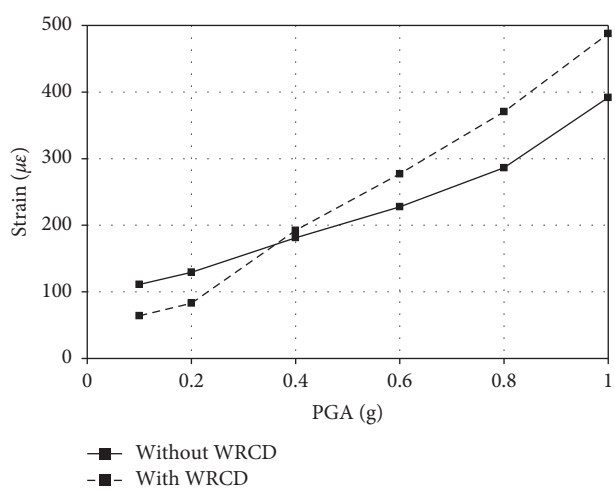

Figure 16: Maximum strain response at 1# sliding pier bottom.

of EL Centro. For sliding bearing piers, when the peak acceleration was 0.1–0.4 g, the maximum strain response value with WRCD was slightly lower than that without WRCD and the average reduction range was 30%. When the peak acceleration was 0.4 g, the two were close and the variation range was 7%. When the peak acceleration was 0.6–1.0 g, the maximum strain response value of the pier bottom of each pier with WRCD greatly increased than that without WRCD, and the average increase range was 50%. For the maximum strain response value of 2# fixed bearing pier bottom, the value with WRCD was lower than that without WRCD and the maximum decrease was 36% when the peak acceleration was 1.0 g.

From the variation trend of the curve, the maximum strain response at the bottom of each pier linearly changed with the seismic input intensity. For the sliding bearing piers without WRCD, the variation trend of the maximum strain response at the pier bottom with the seismic input strength was relatively low, whereas, with WRCD, the variation trend of the maximum strain response at the pier bottom with the seismic input strength was relatively steep. This indicated

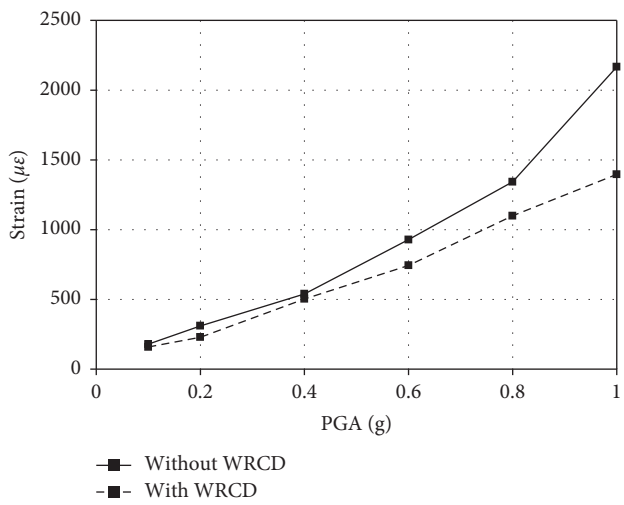

Figure 17: Maximum strain response at 2# fixed pier bottom.

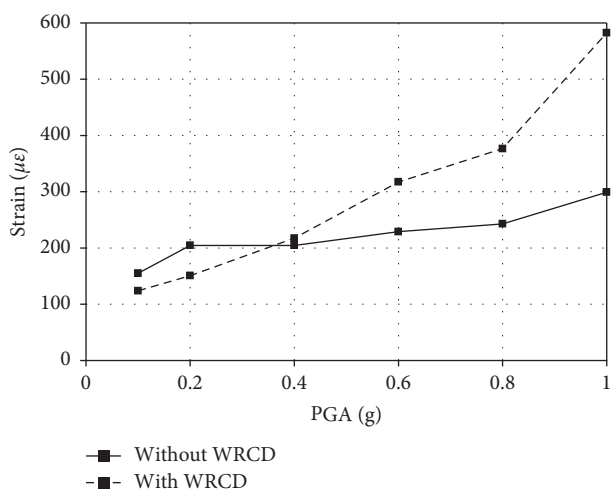

Figure 18: Maximum strain response at 3# sliding bearing pier bottom.

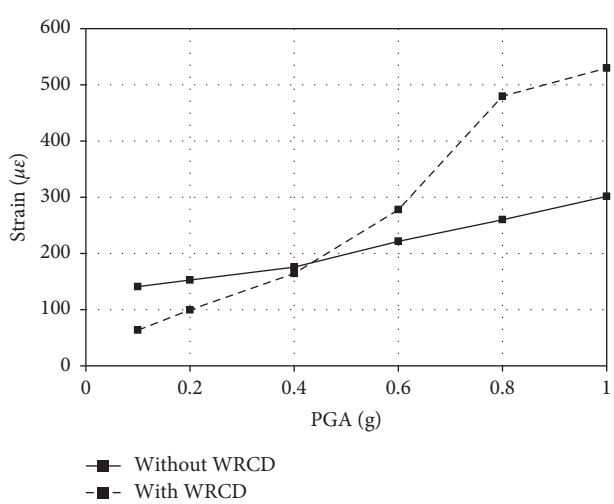

Figure 19: Maximum strain response at 4# sliding pier bottom.

that when the WRCD is activated, the sliding bearing piers contribute to the longitudinal force of the structure and share part of the inertial force of the main beam. Furthermore, with an increase in seismic input intensity, the seismic response of the fixed-bearing pier was reduced further, and the synergistic force effect of each pier was more prominent.

4.5. Responses for Different Frequency Spectra. Table 5 presents the peak acceleration response values of the sliding bearing pier with and without WRCD with different ground motion characteristics under four typical site conditions when the peak acceleration is 0.4 g. Owing to the Tian Jin ground motion of the Class IV site, the data collected without the WRCD test are wrong; hence, the value is not listed in the table. For the Qian An ground motion of Class I site, EL Centro ground motion of the Class II site, and Taft ground motion of the Class III site, the maximum acceleration response value of sliding bearing piers with WRCD with the same parameters was reduced and the reduction range was close. The maximum acceleration response value of the fixed bearing pier increased and the increased range was different. Under the seismic input of EL Centro in the Class II site and Taft in the Class III site, the increased amplitude was 4.6 and 7.8 times, respectively. However, under the Qian An ground motion of the Class I site, the increased amplitude was only 17.5%. The WRCD can effectively improve the cooperative force state between sliding bearing piers and fixed bearing pier of continuous girder bridges; however, the improvement result is directly associated with the ground motion characteristics.

Table 6 shows the comparison values of displacement responses of the pier top and main beam when the peak acceleration is 0.4 g under typical four site conditions with different ground motion characteristics. Under the seismic input of EL Centro in the Class II site, Taft in the Class III site, and Tian Jin in the Class IV site, the maximum displacement response value of sliding bearing piers increased with WRCD for the same setting parameters. Under the seismic input of EL Centro in the Class II site and Taft in the Class III site, the maximum increase in the amplitude of displacement response of sliding bearing piers was ~30%. Under the seismic input of Tian Jin in the Class IV site, the displacement of sliding bearing piers significantly increased (up to approximately two times). For the looser site, the displacement amplification effect of WRCD for sliding bearing piers was more prominent. For the displacement of the main beam, the variation rule was similar to the displacement of the sliding bearing piers. Compared to without WRCD, the maximum displacement response value of the main beam decreased and the decrease was more substantial under the seismic input of EL Centro in the Class II site and Taft in the Class III site and slightly reduced under the seismic input of Tian Jin in Class IV site.

Under the seismic input of Qian An ground motion in the Class I site, the performance of WRCD was not as considerable as that in other sites. However, the variation

Table 5: Maximum acceleration for different frequency spectra (g).

Peak acceleration (g)	Location	Qian An (I)			EL Centro (II)			Taft (III)			Tian Jin (IV)		
		Without WRCD 1	With WRCD 2	Relative error (2 − 1)/1	Without WRCD 1	With WRCD 2	Relative error (2 − 1)/1	Without WRCD 1	With WRCD 2	Relative error (2 − 1)/1	Without WRCD 1	With WRCD 2	Relative error (2 − 1)/1
0.4	P1	0.917	0.954	4.0%	1.563	1.447	−7.4%	1.669	1.674	0.3%	—	2.249	—
	P2	0.109	0.128	17.5%	0.147	0.824	459.2%	0.121	1.063	776.3%	—	1.876	—
	P3	1.304	1.043	−20.0%	1.366	1.014	−25.8%	1.915	1.891	−1.2%	—	2.664	—
	P4	0.82	0.761	−7.1%	1.384	1.281	−7.4%	1.778	1.547	−13.0%	—	2.208	—

Table 6: Maximum displacement for different frequency spectra (mm).

Peak acceleration (g)	Location	Qian An (I)			EL Centro (II)			Taft (III)			Tian Jin (IV)		
		Without WRCD 1	With WRCD 2	Relative error (2 − 1)/1	Without WRCD 1	With WRCD 2	Relative error (2 − 1)/1	Without WRCD 1	With WRCD 2	Relative error (2 − 1)/1	Without WRCD 1	With WRCD 2	Relative error (2 − 1)/1
0.4	P1	0.117	0.078	−33.4%	2.707	2.777	2.6%	2.653	3.355	26.4%	2.845	8.662	204.5%
	P2	0.161	0.349	117.4%	8.876	7.570	−14.7%	10.951	8.621	−21.3%	23.205	23.153	−0.2%
	P3	0.110	0.422	283.9%	2.505	3.333	33.1%	2.802	3.638	29.8%	3.652	10.057	175.4%
	P4	0.569	0.451	−20.8%	3.038	3.557	17.1%	4.319	4.255	−1.5%	3.686	10.796	192.9%

Table 7: Maximum strain response for different frequency spectra ($\mu\varepsilon$).

Peak acceleration (g)	Location	Qian An (I)			EL Centro (II)			Taft (III)			Tian Jin (IV)		
		Without WRCD 1	With WRCD 2	Relative error (2 − 1)/1	Without WRCD 1	With WRCD 2	Relative error (2 − 1)/1	Without WRCD 1	With WRCD 2	Relative error (2 − 1)/1	Without WRCD 1	With WRCD 2	Relative error (2 − 1)/1
0.4	P1	64.09	59.21	−7.6%	181.28	192.27	6.1%	187.99	221.56	17.9%	211.80	482.19	127.7%
	P2	100.71	109.86	9.1%	538.96	502.95	−6.7%	650.05	580.46	−10.7%	1466.72	1416.06	−3.5%
	P3	96.44	97.66	1.3%	204.47	217.29	6.3%	229.50	247.20	7.7%	274.06	543.23	98.2%
	P4	95.83	62.87	−34.4%	175.79	164.19	−6.6%	185.55	198.98	7.2%	247.20	493.79	99.8%

rule was slightly different. Under some site conditions, the WRCD can effectively improve the cooperative force state between sliding bearing piers and fixed bearing piers; however, the improvement result was directly associated with the ground motion characteristics.

Table 7 shows the comparison of maximum strain response at the bottom of each pier with different ground motion characteristics under four typical site conditions when the peak acceleration is 0.4 g. Similar to the displacement response, for the seismic input of EL Centro in the Class II site, Taft in the Class III site, and Tian Jin in the Class IV site, the maximum strain response value of sliding bearing piers, with WRCD with the same setting parameters, increased. Under the seismic input of EL Centro in the Class II site and Taft in the Class III site, the maximum increased amplitude of strain response of sliding bearing piers was 20%. Under the seismic input of Tian Jin in the Class IV site, the strain response of sliding bearing piers significantly increased, up to 1.2 times. The maximum strain response at the pier bottom of the fixed bearing pier decreased, and the maximum reduction in the three types of sites was 10%.

This result demonstrates that, under some site conditions, same as the displacement response, the WRCD can effectively improve the synergistic effect between the sliding bearing piers and the fixed bearing pier; however, the improvement result is directly associated with the seismic input characteristics.

5. Conclusions

This article proposed the WRCD based on the basic principle of cooperative force and considered the relative acceleration of piers and beams as the control variable. The shaking table test of a typical continuous girder bridge was conducted to examine the seismic reduction performance of the WRCD for the continuous girder bridges. Based on the tests, the results demonstrated the following observations:

(1) When the peak acceleration was 0.4 g, the natural frequency with WRCD increased, which shows that with the change in ground motion input intensity, the WRCD is activated such that the dynamic characteristics of the bridge structure changes, and the overall performance of continuous girder bridge can be improved.

(2) After the WRCD was activated, the maximum acceleration response value of each sliding bearing pier decreased by 25%, and the maximum acceleration response value of the fixed bearing pier increased by ~4.6 times, which is from 10% to 57% of the maximum response value of the pier with the sliding bearing pier.

(3) When the peak acceleration was between 0.1 and 0.4 g, the difference between the maximum displacement response values of the two models was small. When the peak acceleration was 0.6~1.0 g, compared to without WRCD, the maximum displacement response value of piers with WRCD rapidly increased with the change in seismic input intensity and the maximum displacement difference between the two models was large. When the WRCD was activated, the sliding bearing piers participated in the longitudinal force of the structure and share part of the inertial force of the main beam. With the increase in seismic input intensity, the performance of WRCD was more considerable and the overall performance of the continuous girder bridge can be improved.

(4) From the variation trend of the curve, the maximum strain response at the bottom of each pier changed linearly with the seismic input intensity. For the sliding bearing piers without the device, the variation trend was relatively gentle, and when the WRCD was activated, it was relatively steep. With increasing seismic input intensity, the seismic response of the fixed bearing was is further reduced, and the synergistic force effect of each pier was more considerable.

(5) This article compared the acceleration, displacement, and strain responses of the structure with different ground motion characteristics under four typical site conditions when the peak acceleration was 0.4 g. Under some site conditions, WRCD can effectively improve the cooperative force state between sliding bearing piers and fixed bearing piers; however, the improvement result was directly associated with the ground motion characteristics. It is necessary to determine the design parameters of the WRCD according to the different site conditions, and the optimum application range of the WRCD has been determined.

Data Availability

The data used to support the findings of this study are included within the article.

Conflicts of Interest

The authors declare that they have no conflicts of interest.

Acknowledgments

The authors would like to thank the workers, foremen, and safety coordinators of the main contractors for their participation. This work was supported by the National Natural Science Foundation of China (grant no. 51778022).

References

[1] C. F. Wang, X. C. Chen, and X. S. Xia, "Parameters analysis of the vibration distributing effect of longitudinal displacement limited continuous beam bridges," *Earthquake Engineering and Engineering Vibration*, vol. 32, no. 5, pp. 119–126, 2012.

[2] N. P. Kataria and R. S. Jangid, "Seismic protection of the horizontally curved bridge with semi-active variable stiffness damper and isolation system," *Advances in Structural Engineering*, vol. 19, no. 7, pp. 1103–1117, 2016.

[3] L. Y. Lu and C. C. Hsu, "Experimental study of variable-frequency rocking bearings for near-fault seismic isolation," *Engineering Structures*, vol. 46, pp. 116–129, 2013.

[4] A. Kashiwazaki, M. Tanaka, N. Tokuda, and T. Enomoto, "The earthquake and microtremor isolation floor system utilizing air springs and laminated rubber bearings," *TRANSACTIONS OF THE JAPAN SOCIETY OF MECHANICAL ENGINEERS Series C*, vol. 55, no. 512, pp. 847–852, 1989.

[5] L. P. Ren, S. H. He, H. Y. Yuan, and Z Zhu, "Seismic fragility analysis of bridge system based on fuzzy failure criteria," *Advances in Civil Engineering*, vol. 2019, Article ID 3592972, 13 pages, 2019.

[6] H. X. Jia, J. Q. Lin, and J. L. Liu, "Bridge seismic damage assessment model applying artificial neural networks and the random forest algorithm," *Advances in Civil Engineering*, vol. 2020, Article ID 6548682, 13 pages, 2020.

[7] F. W. Wu, J. F. Luo, W. Zheng et al., "Performance-based seismic fragility and residual seismic resistance study of a long-span suspension bridge," *Advances in Civil Engineering*, vol. 2020, Article ID 8822955, 16 pages, 2020.

[8] L. Tang, Z. H. Cheng, X. Z. Ling, S. Cong, and J. Nan, "Preparation and performance of graphene oxide/self-healing microcapsule composite mortar," *Smart Materials and Structures*, vol. 31, no. 2, Article ID 025022, 2022.

[9] J. M. Kelly and J. M. Eidinger, *Experimental Results of an Earthquake Isolation System Using Natural Rubber Bearings*, Reports No. UCBIEERC78l03, California, CA, USA, 1978.

[10] J. M. Kelly, "Tension buckling in multilayer elastomeric bearings," *Journal of Engineering Mechanics*, vol. 129, no. 12, pp. 1363–1368, 2003.

[11] R. G. Tyler and W. H. Robinson, "High-strain tests on lead-rubber bearings for earthquake loadings," *Bulletin of the New Zealand Society for Earthquake Engineering*, vol. 17, no. 2, pp. 90–105, 1984.

[12] J. S. Hwang, J. M. Chiou, L. H. Sheng, and J. H Gates, "A refined model for base-isolated bridges with Bi-linear hysteretic bearings," *Earthquake Spectra*, vol. 12, no. 2, pp. 245–273, 1996.

[13] M. Abe, J. Yoshida, and Y. Fujino, "Multiaxial behaviors of laminated rubber bearings and their modeling. I: experimental study," *Journal of Structural Engineering*, vol. 130, no. 8, pp. 1119–1132, 2004.

[14] T. B. Peng, J. Z. Li, and L. C Fan, "Analysis of vertical displacement of double spherical aseismic bearing," *J. Tung-chi Univ., Nat. Sci*, vol. 35, no. 9, pp. 1181–1185, 2007.

[15] Y. L. Zhang, Y. J. Zhang, and C. F. Wang, "Effect of vertical ground motion on seismic response of an isolated bridge with FPS," *J. Lanzhou Jiaotong Univ*, vol. 31, no. 1, pp. 18–22, 2012.

[16] J. P. Ou and B. Wu, "Experimental comparison on the properties of friction and mild steel yielding energy dissipations and their effects on reducing vibration of structure under earthquakes," *Earthquake. Eng. Eng. Dyn*, vol. 3, pp. 73–87, 1995.

[17] W. M. Yan, Y. Li, and Y. J. Chen, "The implication of a new type of metal alloy brace on seismic control of viaduts," *Journal of Beijing University of Technology*, vol. 38, no. 8, pp. 1167–1173, 2012.

[18] X. Shen, X. B. Ni, and A. J. Ye, "A new type of metallic damper for birdges aseismic performance in transverse direction," *Journal of Vibration and Shock*, vol. 33, no. 21, pp. 96–101, 2014.

[19] Z. H. Cheng and Y. S. Deng, "Bearing characteristics of moso bamboo micropile-composite soil nailing system in soft soil areas," *Advances in Materials Science and Engineering*, vol. 2020, Article ID 3204285, 17 pages, 2020.

[20] Y. S. Deng, Z. H Cheng, M. Z. Cai, Y Sun, and C Peng, "An experimental study on the ecological support model of dentate row piles," *Advances in Materials Science and Engineering*, vol. 2020, Article ID 6428032, 12 pages, 2020.

[21] X. S. Liu, W. Guo, J. Z. Li, and H Zhang, "Seismic study of skew bridge supported on laminated-rubber bearings," *Advances in Civil Engineering*, vol. 2020, Article ID 8899693, 17 pages, 2020.

[22] Y. T. Pang, "Seismic fragility assessment of an isolated multipylon cable-stayed bridge using shaking table tests," *Advances in Civil Engineering*, vol. 2017, Article ID 9514086, 12 pages, 2017.

[23] H. X. Gao, Y. Song, W. T. Yuan, H Lu, and S Cao, "Seismic design method of self-centring-segment bridge piers with tensile-type viscoelastic dampers," *Advances in Civil Engineering*, vol. 2021, Article ID 6688006, 12 pages, 2021.

[24] C. Zou, J. A. Moore, M. Sanayei, Z. Tao, and Y. Wang, "Impedance model of train-induced vibration transmission across a transfer structure into an over track building in a metro depot," *Journal of Structural Engineering*, vol. 148, no. 11, Article ID 04022187, 2022.

[25] H. Jin, Q. Tian, and Z Li, "Crack development of rebar rust in rubberized concrete using mesoscale model," *Construction and Building Materials*, vol. 321, Article ID 126409, 2022.

[26] L. H. Xu and M. Ma, "Dynamic response of the multilayered half-space medium due to the spatially periodic harmonic moving load," *Soil Dynamics and Earthquake Engineering*, vol. 157, Article ID 107246, 2022.

[27] Y. Pang, K. Wei, H. He, and W. Wang, "Assessment of lifetime seismic resilience of a long-spancable-stayed bridge exposed to structural corrosion," *Soil Dynamics and Earthquake Engineering*, vol. 157, Article ID 107275, 2022.

[28] Y. Pang and X. Wang, "Cloud-IDA-MSA conversion of fragility curves for efficient and high-fidelity resilience assessment," *Journal of Structural Engineering*, vol. 147, no. 5, Article ID 4021049, 2021.